Quantum vortex melting and phase diagram in the layered organic superconductor κ-(BEDT-TTF)$_2$Cu(NCS)$_2$

S. Uji, Y. Fujii, and S. Sugiura
National Institute for Materials Science, Tsukuba, Ibaraki 305-0003, Japan
and Graduate School of Pure and Applied Sciences, University of Tsukuba, Tsukuba, Ibaraki 305-8577, Japan

T. Terashima and T. Isono
National Institute for Materials Science, Tsukuba, Ibaraki 305-0003, Japan

J. Yamada
Graduate School of Material Science, University of Hyogo, Hyogo 650-004, Japan

(Received 4 November 2017; revised manuscript received 18 December 2017; published 8 January 2018)

Resistance and magnetic torque measurements have been performed to investigate vortex phases for a layered organic superconductor κ-(BEDT-TTF)$_2$Cu(NCS)$_2$ [BEDT-TTF = bis(ethylenedithio)tetrathiafulvalene], which is modeled as stacks of Josephson junctions. At 25 mK, the out-of-plane resistivity increases at 0.6 T, has a step feature up to 4 T, and then increases again, whereas the in-plane resistivity monotonically increases above 4 T. The results show that both pancake vortices (PVs) and Josephson vortices (JVs) are in solid phases for $\mu_0 H < 0.6$ T, but only JVs are in a liquid phase for $0.6 < \mu_0 H < 4$ T. For $\mu_0 H > 4$ T, both PVs and JVs are in liquid phases. These melting transitions are predominantly induced by quantum fluctuations (not by thermal fluctuations). In the magnetic torque curves, the irreversibility transition is clearly observed, roughly corresponding to the melting transition of the PVs but no anomaly is found at the JV melting transition. The detailed vortex phase diagram is determined in a wide temperature region.

DOI: 10.1103/PhysRevB.97.024505

I. INTRODUCTION

Superconducting vortices can be viewed as nonsuperconducting (normal) cores surrounded by circulating superconducting (SC) currents. The vortices behave like particles with repulsive interaction, because of which they are called vortex matter. So far, the vortex matter has extensively been studied because of fascinating phenomena especially for highly two-dimensional (2D) layered superconductors [1,2]. In layered superconductors such as high T_c cuprates or organics, the perpendicular Ginzburg-Landau (GL) coherence length is comparable to the SC layer spacing. Therefore, these layered superconductors can be modeled as stacks of Josephson junctions. When a magnetic field is applied perpendicular to the layer, the flux lines penetrating the SC layers form pancake vortices (PVs) in the individual layers [Fig. 1(a)], whose core radius is given by the in-plane coherence length $\xi_\parallel$. These PVs are pinned at some inhomogeneity in the layers, where the SC order parameter is reduced. At sufficiently low temperatures and low fields, the SC layers are strongly Josephson coupled and the flux lines straightly penetrate the SC layers. The PVs form an elastically disordered lattice but almost a three-dimensional (3D) regular lattice as depicted in Fig. 1(a). This vortex phase is called Bragg glass (BG). As the field increases, the Josephson coupling weakens and the disorder effect is effectively enhanced (the pinning energies overcome the vortex elastic energy), and then entangled flux lines are formed [3]. A disordered 2D lattice structure remains in each SC layer but has no structural correlation between the SC layers. This phase is called vortex glass (VG) [Fig. 1(b)]. At the BG-VG transition, the vortex pinning energies play an essential role [4–6]. Because of the entangled structure in the VG phase, the flux lines are kinked between the SC layers, where Josephson vortices (JVs) are formed. As the field further increases, the VG will melt, where both PVs and JVs are highly fluctuating.

Due to repulsive interaction between vortices, the vortex in a solid phase is modeled as a particle in a confinement potential [Fig. 1(c)]. The mean-square amplitude of the vortex fluctuation will be given by $\langle u^2 \rangle = \langle u_T^2 \rangle + \langle u_Q^2 \rangle$, where $\langle u_T^2 \rangle$ and $\langle u_Q^2 \rangle$ are due to thermal fluctuations (TF) and quantum fluctuations (QF), respectively. The TF are characterized by the Ginzburg number $Gi = [T_c/H_c^2(0)\epsilon]\xi_\parallel(0)^3]^2$, where H_c is the thermodynamic critical field, ϵ is the effective mass ratio, $\epsilon = m/M = H_{c2\perp}/H_{c2//}$, and $\xi_\parallel(0)$ is the in-plane coherence length at zero temperature. The QF are characterized by the ratio of the normal state sheet resistivity of each layer to quantum resistance $Q = (e^2/\hbar)\rho_N/s$, where s is the layer spacing. As temperature increases, the fluctuation amplitude $\langle u_T^2 \rangle$ is enhanced and the vortex solid will melt at a certain temperature, which is a thermal melting (TM) transition. On the other hand, as the field increases, the lattice constant $a_0 \propto \sqrt{\phi_0/H}$ decreases, where ϕ_0 is the flux quantum. When a_0 becomes comparable to $\langle u^2 \rangle$, the vortex solid will melt. This melting transition takes place even at zero temperature; it is a quantum melting (QM) transition [7–10]. The critical value giving the melting transition, the so-called Lindemann criterion

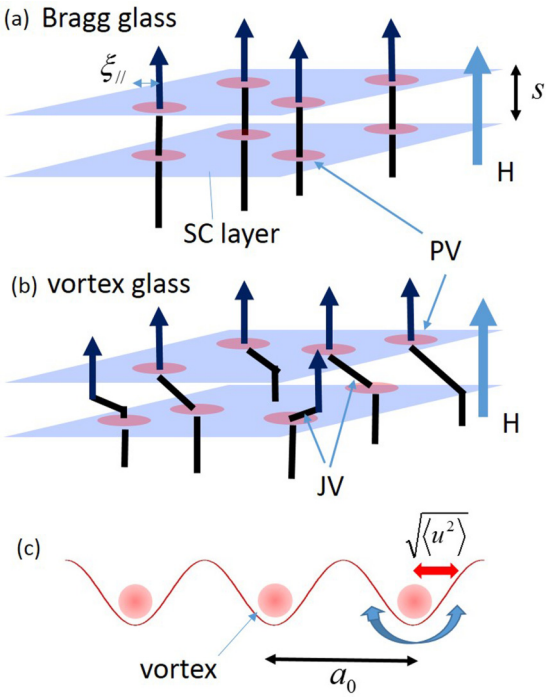

FIG. 1. Schematics of flux lines in (a) Bragg and (b) vortex glass phases. In Bragg glass phase, each flux line straightly penetrates the SC layers. Only PVs are formed. In vortex glass phase, flux lines fluctuate and kinked in the insulating layers, forming JVs. (c) Schematic of vortices and their confinement potential. $\sqrt{\langle u^2 \rangle}$ represents the mean square displacement of a vortex.

c_L, defined by $\langle u^2 \rangle / a_0^2 = c_L^2$, is estimated as $c_L = 0.1$–0.3 by Monte Carlo simulations [11].

Although extensive studies of vortices have been made in layered superconductors [12–15], the melting transition has been discussed only for the PVs so far. In the VG phase, the entangled flux line structures inevitably lead to JV formation between the SC layers [Fig. 1(b)] [16]. The JVs, which are pinned in the insulating layers very weakly, will be fluctuating much more than the PVs. Therefore, we could expect characteristic dynamics of JVs as well as PVs.

We have measured in-plane and out-of-plane resistivities, and magnetic torque in a wide temperature and field range for a layered organic superconductor κ-(BEDT-TTF)$_2$Cu(NCS)$_2$ [17]. We report that QF of the JVs cause peculiar energy dissipations at low temperatures, and provide strong indications showing that the PVs and JVs melt separately.

II. EXPERIMENTS

κ-(BEDT-TTF)$_2$Cu(NCS)$_2$ has a layered structure, composed of conducting BEDT-TTF and insulating Cu(NCS)$_2$ layers [Fig. 2(a)]. Single crystals of κ-(BEDT-TTF)$_2$Cu(NCS)$_2$ were prepared by electrochemical oxidation in an appropriate solvent. The crystals have platelike shapes, whose typical sizes are $600 \times 200 \times 50$ μm^3 for resistance and $200 \times 100 \times 20$ μm^3 for torque measurements. For the resistance measurements, six gold wires (ϕ 10 μm) were attached on both sides of the crystal (conducting bc plane) by carbon

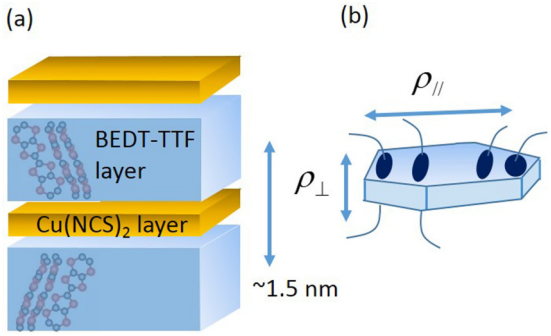

FIG. 2. (a) Schematic structure of κ-(BEDT-TTF)$_2$Cu(NCS)$_2$. (b) Schematic of single crystal and electric contact configuration.

paste [Fig. 2(b)]. The sample voltage V was measured by a conventional four-probe ac technique with electric current I parallel and perpendicular to the conducting plane. The resistance is defined as $R = V/I$. The magnetic torque was measured by a microcantilever technique [18]. All the samples are slowly cooled from room temperature to 4.2 K at a rate of 0.5 K/min to minimize the effect of the structural instabilities, which is likely related to ethylene group disorders of the BEDT-TTF molecules [19]. The experiments were performed by superconducting magnet systems at Tsukuba magnet laboratory, NIMS.

III. RESULTS

Figures 3(a) and 3(b) present the field dependence of the in-plane ($\rho_\parallel$) and out-of-plane resistivities ($\rho_\perp$) at 25 mK, respectively. The in-plane resistivity is below the noise level at low fields, but rapidly increases above 4 T and then has a tendency to saturate above 8 T. Above 10 T, Shubnikov–de Haas (SdH) oscillations are observed [inset of Fig. 3(a)]. The out-of-plane resistivity first rapidly increases above ~0.6 T, has a step for $0.6 < \mu_0 H < 4$ T, and then increases again [Fig. 3(b)]. The SdH oscillations are also observed at high fields. Both resistivities slightly depend on the current density (j) up to ~8 T, likely due to vortex dynamics. No current dependence above 8 T suggests that the SC state is completely broken, $H_{c2\perp} \sim 8$ T. This $H_{c2\perp}$ value is sample dependent and higher than the previous report (~7 T) [14]. Although this definition may overestimate $H_{c2\perp}$, our conclusions are not affected by this ambiguity. The $H_{c2\perp}$ values above 3 K are consistent with magnetic susceptibility measurements [20]. At higher current densities, we note that the SdH oscillations are suppressed (not shown), probably due to joule heating. The large difference between $\rho_\parallel(H)$ and $\rho_\perp(H)$ suggests that vortex dynamics plays an essential role as discussed later. Here we define three vortex phases I–III. Region I ($\mu_0 H < 0.6$ T): $\rho_\parallel = 0$ and $\rho_\perp = 0$. Region II ($0.6 < \mu_0 H < 4$ T): $\rho_\parallel = 0$ and $\rho_\perp > 0$. Region III (4 T $< \mu_0 H < H_{c2}$): $\rho_\parallel > 0$ and $\rho_\perp > 0$.

The step behavior of $\rho_\perp$ in region II is sample dependent. In Fig. 4, $\rho_\perp$ curves are presented for two other samples (R2 and R3). For R2, the $\rho_\perp$ value in region II slightly decreases with increasing temperature. For R3, the $\rho_\perp$ value in region II is much lower and has stronger field dependence. At a low current density, the resistivity decreases down to the noise level around 4 T. These results show that the step behavior

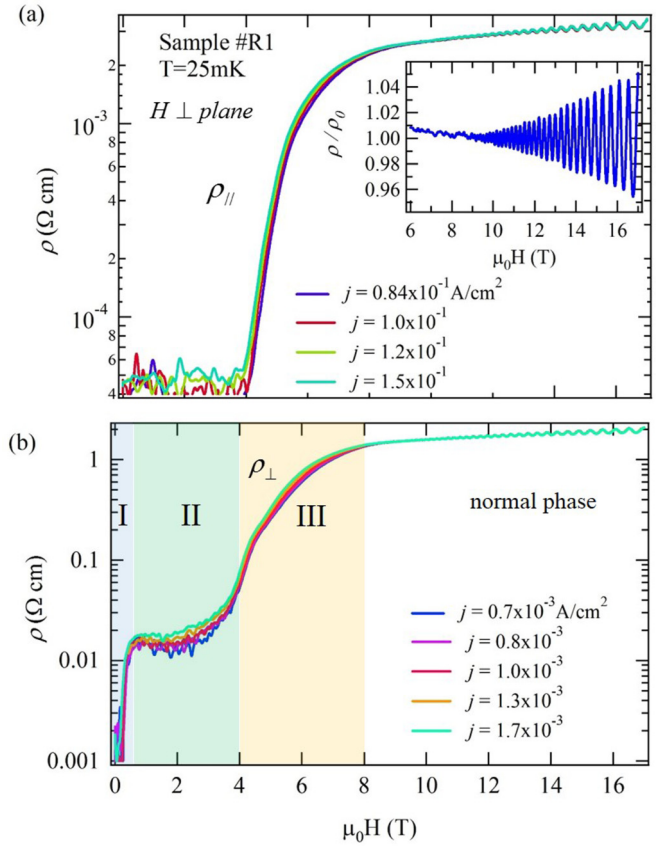

FIG. 3. Magnetic field dependence of (a) in-plane ($\rho_{//}$) and (b) out-of-plane resistivities ($\rho_\perp$) at 25 mK at various current densities. The vortex phase can be divided into three regions I, II, and III. Inset: SdH oscillations normalized by a nonoscillatory part (ρ_0).

depends on the sample quality. However, the step region is almost independent of the sample. From the field dependence of the SdH oscillations, we obtain the Dingle temperatures $T_D = 0.8$–1.4 K. Although T_D is a good measure of the sample

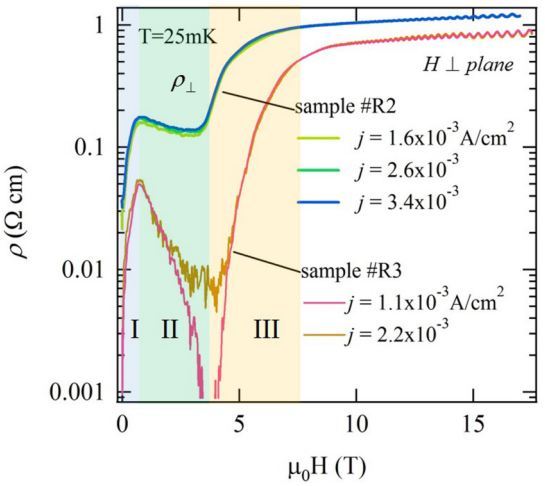

FIG. 4. Magnetic field dependence of out-of-plane resistivities ($\rho_\perp$) for samples R2 and R3.

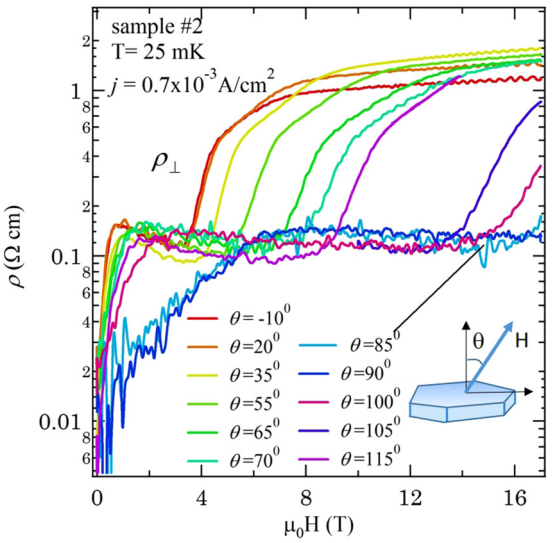

FIG. 5. $\rho_\perp(H)$ curves at various field angles for samples R2.

quality, we see no significant correlation between the T_D and step resistivities.

Figure 5 presents the field dependence of the out-of-plane resistivity at various field angles. When the field is nearly perpendicular to the layer, the step is observed in the range between 0.7 and 3.5 T. This field range (region II) shifts to high fields as the field is tilted from the perpendicular direction. We observe the step behavior in a wide range between 6 and 16.5 T for $\theta = 85°$. An interesting feature is that the step value is almost constant (independent of the field direction.)

Figure 6 presents the angular dependence of the characteristic fields H_{s1}, H_{s2}, and H_{c2} obtained from the $\rho_\perp(H)$ curves (Fig. 5), which are defined in the inset. All these fields increase as the field is tilted from the perpendicular to parallel direction. We note that H_{s1} has a maximum value ~7 T for $\theta = 90°$ but the others exceed 18 T for $\theta \approx 90°$. The angular dependence of H_{c2} at 1.56 K [21] is well reproduced by the 2D Tinkham

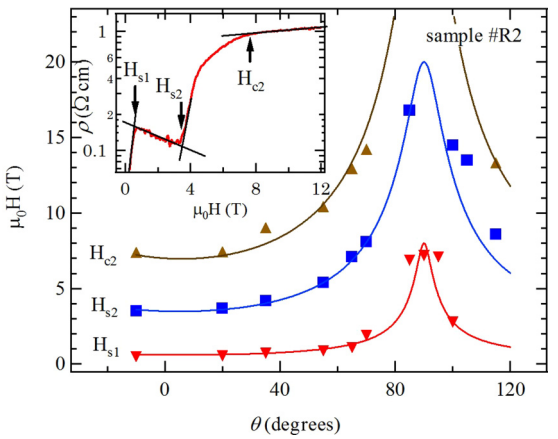

FIG. 6. Angular dependence of characteristic fields H_{s1}, H_{s2}, and H_{c2} at 25 mK. Inset: Definition of H_{s1}, H_{s2}, and H_{c2}. The solid curves are the fitted results with Eq. (1).

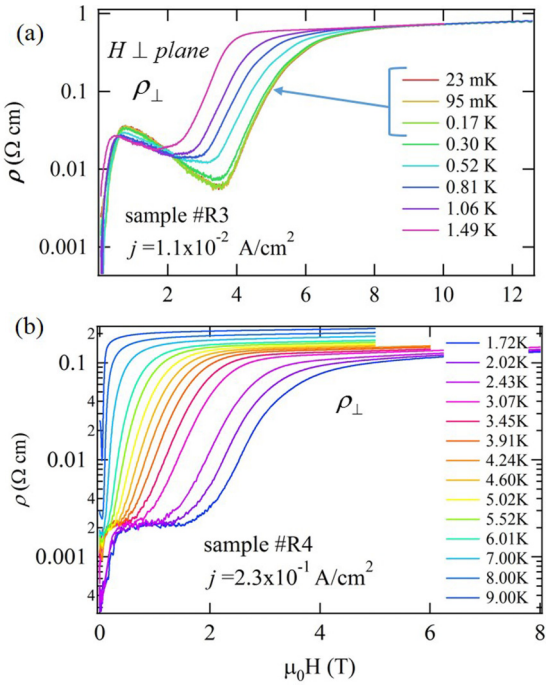

FIG. 7. Magnetic field dependence of $\rho_\perp$ at various temperatures for samples (a) R3 and (b) R4.

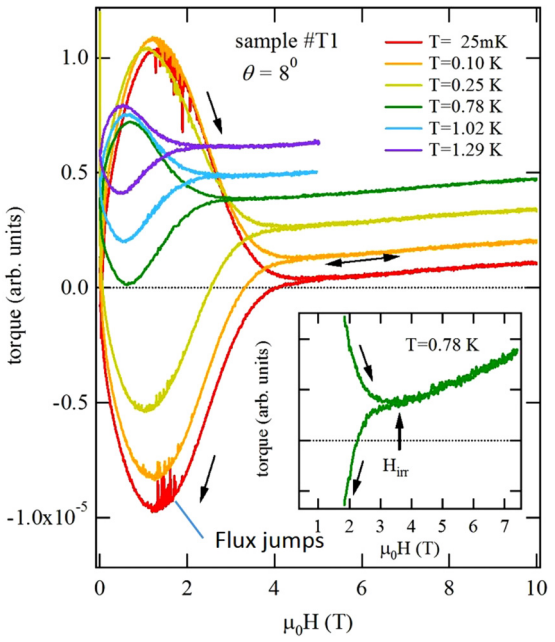

FIG. 8. Magnetic torque curves at various temperatures. Each curve is shifted for clarity.

model [22],

$$\left|\frac{H_{c2}(\theta)\cos(\theta)}{H_{c2\perp}}\right| + \left\{\frac{H_{c2}(\theta)\sin(\theta)}{H_{c2\parallel}}\right\}^2 = 1. \quad (1)$$

The $H_{s2}(\theta)$ data in Fig. 6 are also fitted with this model. The solid curve in Fig. 6 shows the calculated results for $H_{c2\perp} = 7$ T and $H_{c2\parallel} = 35$ T [23]. These values are much larger than those at 1.56 K, $H_{c2\perp} = 2.3$ T and $H_{c2\parallel} = 24.5$ T [21]. Similarly, $H_{s1}(\theta)$ and $H_{s2}(\theta)$ can roughly be reproduced by the same model, where $H_{s1\perp} = 0.6$ T, $H_{s1\parallel} = 8$ T, $H_{s2\perp} = 3.5$ T, and $H_{s2\parallel} = 20$ T.

Figure 7 presents $\rho_\perp(H)$ curves at various temperatures. Region II monotonically decreases with increasing temperature and the step feature is not evident above ~5 K. The step value is almost independent of temperature although the normal state resistivity at high fields increases with increasing temperature.

Figure 8 presents the magnetic field dependence of the torque at various temperatures. The torque τ is given by $\tau = \mu_0 M \times H$, where μ_0 is the permeability of vacuum. The field is slightly tilted from the perpendicular direction to obtain a large torque signal. The overall behavior is consistent with previous results [12,13]. Because of strong pinning of the PVs in the SC layers, we observe large hysteresis in a wide field region. As temperature increases, the torque hysteresis is reduced and the hysteresis region shrinks. As indicated in the inset, we can define the irreversibility field $H_{\rm irr}$, above which the torque becomes reversible. It is not easy to define H_{c2} ($>H_{\rm irr}$) from the torque measurements because of the smooth variation above $H_{\rm irr}$. At low temperatures, many spikes due to flux jumps are observed in the range between 1.5 and 2 T.

The phase diagram determined from the resistivity and torque measurements is presented in Fig. 9(a). Since the lower critical field H_{c1} is only ~0.002 T [24], a little amount of the magnetic flux is excluded from the sample in the field region where we discuss here. In Fig. 9(b) we note that $H_{\rm irr}$ is significantly larger than H_{s2} below 1 K. The temperature dependence of H_{s1} has a kink at 0.5 K as indicated by an arrow in Fig. 9(c).

IV. DISCUSSION

A. Phase diagram

In region I we observe $\rho_\parallel = 0$ and $\rho_\perp = 0$ (Fig. 3), showing that all the vortices are pinned and not driven by the currents. Therefore, region I can be assigned to the BG phase. In the BG phase, the SC layers are strongly Josephson coupled and the PVs form a disordered 3D lattice [Fig. 1(a)]. Therefore, all the flux lines are collectively pinned, suggesting a large depinning current.

In region II the results $\rho_\parallel = 0$ but $\rho_\perp > 0$ mean that the JVs are driven by the currents, whereas the PV are pinned in the SC layers. This phase will be assigned to a VG phase [Fig. 1(b)], where the flux lines are entangled. In this region we observe $\rho_\perp > 0$ even at very low current densities, showing that the JVs are in a liquid phase; H_{s1} can be assigned to the quantum melting transition of the JVs. In region III we observe $\rho_\parallel > 0$ and $\rho_\perp > 0$, showing that both PVs and JVs are in a liquid phase. Therefore, H_{s2} is assigned to the quantum melting transition of the PVs. In this way we can conclude that the JVs and PVs show quantum melting transitions separately.

By Monte Carlo simulations with a realistic vortex interaction, the effect of a reconnection of the flux lines between the layers is studied, and it is shown that the reconnection causes a sizable difference of the mean-square amplitude of the PV fluctuations in a liquid phase [11]. The simulations do not directly predict a QM transition of the JVs, but suggest

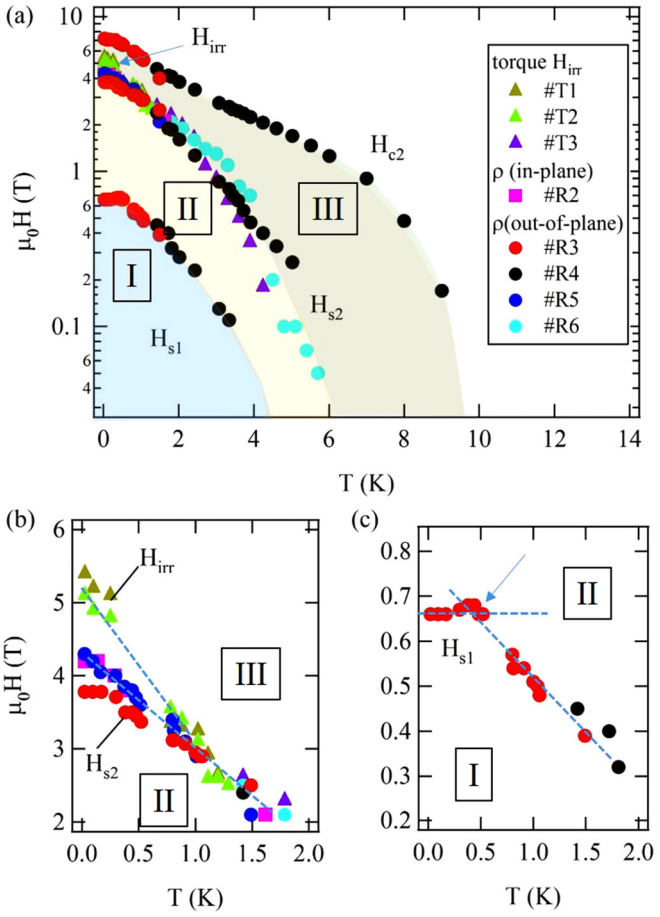

FIG. 9. (a) Magnetic field phase diagram in perpendicular field. H_{irr} is determined from the torque measurements, and H_{s1}, H_{s2}, and H_{c2} are from resistivity measurements. Regions I, II, and III are assigned to BG, VG, and liquid phase, respectively. Low temperature behavior of (b) H_{irr} and H_{s2}, and (c) H_{s1}. Dashed lines are guides for the eye. The arrow in (c) indicates the kink.

that the JV melting is closely related to layer decoupling at the BG-VG transition.

For highly 2D superconductors, diamagnetic torque signal is predominantly caused by the perpendicular diamagnetism of the SC layers [25]. Therefore, the hysteresis of the toque signal arises from the pinning of the PVs but not from the pinning of the JVs. Therefore, it will be reasonable to observe no anomalies at H_{s1} in the torque curves.

For κ-(BEDT-TTF)$_2$Cu(NCS)$_2$, we obtain the Ginzburg number $Gi \approx 0.01$, using $T_c = 9$ K, $\epsilon = 5$, $\xi_{\parallel} = 60$ nm, $H_c = H_{c2}/\sqrt{2}\kappa = 500$ G, and $\kappa = 100$ [24]. This Gi value is comparable to that of a high T_c cuprate $YBa_2Cu_2O_{7-\delta}$ [7]. The parameter $Q^* = Q/\sqrt{Gi}$, showing a relative strength of the quantum fluctuations, gives a crossover from the (high-T) TM regime to (low-T) QM regime [7]. The melting field extrapolates to H_{c2} at $T = 0$ K in the TM regime but it remains below H_{c2} in the QM regime. At the crossover field $H_Q = H_{c2}/(Q^*)^2$, a kink will be observed in the temperature dependence of the melting field [7]. For κ-(BEDT-TTF)$_2$Cu(NCS)$_2$, H_Q is estimated as 0.08–8 T. The large ambiguity arises from the zero field ρ_N value in Q. In the temperature dependence of H_{s2} [Fig. 9(b)], no significant kink is observed. On the other hand, the JV melting field H_{s1} has a kink at 0.5 K in the temperature dependence [Fig. 9(b)]. The kink may suggest a crossover from a TM to QM regime. Since the JVs are formed in the insulating layers, where the order parameter is zero, it is expected that the JVs are highly fluctuating quantum mechanically. This will be the reason of the lower QM field of the JVs than that of the PVs. We should note that H_{s1} does not reach H_{s2} even at the lowest temperature.

B. Comparison with previous results

It is reported that the irreversibility field H_{irr} linearly increases with decreasing temperature down to 0.12 K, which is extrapolated to ~4 T at 0 K [12]. In the torque curve, a kink is observed at ~3.7 T below H_{irr}(~4.2 T) for $T = 25$ mK [13]. This kink is assigned to the melting transition of the PVs. These results are almost consistent with our picture; H_{s2} is the melting field of PVs.

The in-plane resistance shows strong nonlinear dependence below 1 K in region III [14]. A strong dumping of the SdH oscillations is observed in the same region [15]. These results are explained in terms of vortex slush, induced by quantum fluctuations. In our samples, such nonlinear behavior is slightly seen. The T_D values for our samples (0.8–1.4 K) are higher than their values [15], suggesting that our samples have more pinning sites of the vortices. This is probably the reason for no strong nonlinear behavior in region III.

Microwave response measurement in a wide frequency range has reported a Josephson plasma resonance [26], whose resonance field has a cusp as a function of temperature. The cusp field H_{cusp} increases with decreasing temperature, $H_{cusp} \approx 0.2$ T at 3 K and 0.1 T at 4 K. This cusp has been explained in terms of a melting transition of the vortices or a depinning transition. We note that H_{cusp} approximately corresponds to H_{s1}, suggesting that the cusp is caused by the JV melting.

In μSR measurements at 1.8 K, a symmetric μSR line shape is observed at 40 mT, which is not explained by a conventional vortex lattice model [27]. The results are discussed in terms of the loss of the short range correlation of the PVs between the layers. It sounds like a BG-VG transition, but the decoupling field (~40 mT) is much lower than H_{s1} in Fig. 9(c).

Yin *et al.*, measured the interlayer resistance $\rho_{\perp}$ and found that nonzero resistance appears above 4 T at zero field for a high current density [28]. The behavior is interpreted in terms of current and thermally driven phase slips caused by PV motion. The nonzero resistance may be caused by the JV melting. However, only a single phase boundary is present below H_{c2} in their vortex phase diagram, which is different from the results in Fig. 9(a).

An anomalous second peak in the magnetization curves, which shows the enhancement of the PV pinning, is observed at ~0.015 T between 2 and 6 K [29]. This second peak is attributed to the dimensional crossover in the vortex phase. The second peak field is almost independent of temperature, which is neither consistent with H_{s1} nor with H_{s2}.

One of the significant differences of the phase diagram in Fig. 9(a) from the high T_c cuprates will be the temperature dependence of the phase boundary H_{s1}. In high T_c cuprates, the

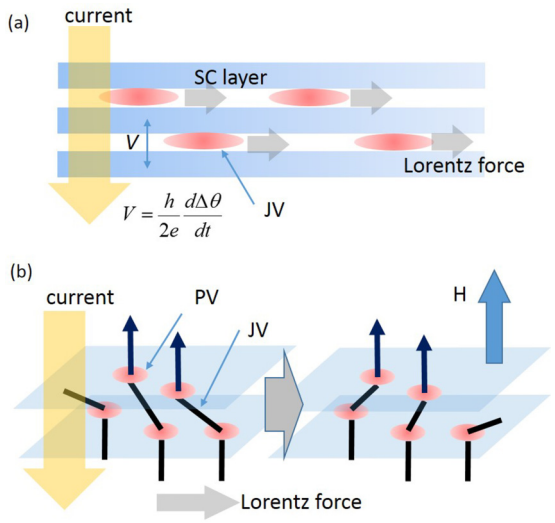

FIG. 10. Schematics of drift motion of JVs in region II. (a) JVs are driven in the layer direction by Lorentz force in perpendicular current. This JV drift motion leads to a finite voltage between the layers, given by the Josephson relation. (b) In entangled flux line structures, each JV is defined in a microscopic region. When the JVs are collectively driven, the flux lines are cut and reconnected since the PVs are pinned in the SC layers.

BG-VG transition field increases with increasing temperature and is terminated at a tricritical point. However, for this salt, H_{s1} rapidly decreases with increasing temperature and no tricritical point is observed; the BG phase does not exist in the range between ~4.5 K and T_c. The results suggest that the Josephson coupling is strongly reduced with increasing temperature as compared with the high T_c cuprates and the JVs are highly fluctuating in this salt.

C. Energy dissipation mechanism

In κ-(BEDT-TTF)$_2$Cu(NCS)$_2$, a jump in the I-V characteristics associated with hysteresis would be observed when the perpendicular current exceeds the Josephson critical current (J_c) as has been observed for high T_c cuprates [30,31]. For $Bi_2Sr_2CaCu_2O_{8+x}$, strong nonlinear I-V characteristics associated with jumps are observed at zero field, which are explained by a series connection model of highly capacitive Josephson junctions [30,31]. The critical current J_c ranges from 100 to 7000 A/cm^2, depending on annealing condition, sample dimension, and T_c. For κ-(BEDT-TTF)$_2$Cu(NCS)$_2$, no such critical behavior has been observed in the I-V characteristics, which suggests that the vortex depinning current is lower than J_c. Once the vortices are driven, the phase coherence between the layers is broken, which will vanish the Josephson critical behavior.

In region II, the JVs driven by the current gives the finite voltage between the layers. Microscopically, the energy dissipation due to vortex motion is explained by Josephson relation $d\Delta\theta/dt = eV/\hbar$, where $\Delta\theta$ is the phase difference of the SC state and V is the voltage between the adjacent layers [Fig. 10(a)]. When a JV is driven in an insulating layer from a sample edge to the opposite one, $\Delta\theta$ changes by 2π. Therefore, the voltage in a unit area is given by $V = n_{JV}v_{JV}\phi_0$, where n_{JV} and v_{JV} are the vortex number and velocity, respectively. Since the flux lines are expected to be highly entangled [Fig. 10(b)], we may have $n_{JV} \approx n_{PV}$. At 1 T and 1 mA/cm^2, we estimate $v_{JV} \approx 10^{-6}$ cm/s. This value is eight orders of magnitude smaller than that obtained for a mesa crystal of $Bi_2Sr_2CaCu_2O_{8+x}$ in parallel magnetic fields [31].

The cutting and reconnection processes of the flux lines are required for the drift motion of the JVs [Fig. 10(b)] when the PVs are pinned in the SC layers. The JVs have to be driven from a sample edge to the opposite one to observe the finite voltage. The probability of such collective motion will be very small: only few JVs will be driven. In addition, each JV is defined only in a microscopic region because of the entangled flux line structures. Therefore, the JV drift motion will induce a $d\Delta\theta/dt$ value only in microscopic areas of the SC layers. The voltage contacts spread over ~0.1 × 0.1 mm^2, which will be much larger than the JV length. Therefore, the detected voltage will be averaged out over the contact area.

Finally, we briefly discuss the resistivity behavior in Fig. 4. We see that the resistivity for R3 becomes very small around H_{s2}, showing relatively strong pinning of the JVs or suppression of the JV fluctuation. In the high T_c cuprates, it is reported that the PVs are strongly pinned (the critical current is enhanced) just before the melting transition, showing that the PV fluctuation is suppressed [32,33]. Since each JV is terminated by PVs, it is likely that the suppression of the PV fluctuation will suppress the JV fluctuation, leading to the low resistivity. The sample dependence of the resistivity in region II will be caused by the different pinning site density.

V. SUMMARIES

We have measured the resistance and magnetic torque, and determined the vortex phase diagram for a layered organic superconductor κ-(BEDT-TTF)$_2$Cu(NCS)$_2$, which can be modeled as stacks of Josephson junctions. In magnetic field, the magnetic flux lines are expected to have a characteristic structure, which is composed of PVs in the SC layers and JVs in the insulating layers. At low temperatures we find that the vortex phases are divided into BG, VG, and liquid phases, which are separated by two QM transitions of vortices. As field increases, the JVs melt first, leading to nonzero values only in $\rho_\perp$ and then the PVs melt at a higher field, leading to nonzero $\rho_\parallel$ values. In the torque curves at low temperatures, the irreversibility transition is well defined, corresponding to the QM transition of the PVs. However, no anomaly is found at the JV QM transition in the torque curves, which is probably due to the fact that the torque signal is predominantly determined by the diamagnetic signal of the SC layers. In contrast to high T_c cuprates, a tricritical point of the BG, VG, and liquid phases is not observed at low fields up to ~4 K. The results suggest that the Josephson coupling is strongly reduced with increasing temperature and the JVs are highly fluctuating at high temperatures.

ACKNOWLEDGMENT

This work was supported by a Grant-in-Aid for Scientific Research from MEXT (Grant No. 17H01144).

[1] G. Blatter, M. V. Feigelfman, V. B. Geshkenbein, A. I. Larkin, and V. M. Vinokur, Rev. Mod. Phys. **66**, 1125 (1994).
[2] L. N. Bulaevskii, M. Ledvij, and V. G. Kogan, Phys. Rev. B **46**, 366 (1992).
[3] R. Cubitt, E. M. Forgan, G. Yang, S. L. Lee, D. McK. Paul, H. A. Mook, M. Yethiraj, P. H. Kes, T. W. Li, A. A. Menovsky, Z. Tarnawski, and K. Mortensen, Nature (London) **365**, 407 (1993).
[4] H. Safar, P. L. Gammel, D. A. Huse, G. B. Alers, D. J. Bishop, W. C. Lee, J. Giapintzakis, and D. M. Ginsberg, Phys. Rev. B **52**, 6211 (1995).
[5] T. Giamarchi and P. Le Doussal, Phys. Rev. B **55**, 6577 (1997).
[6] D. T. Fuchs, E. Zeldov, T. Tamegai, S. Ooi, M. Rappaport, and H. Shtrikman, Phys. Rev. Lett. **80**, 4971 (1998).
[7] G. Blatter and B. Ivlev, Phys. Rev. Lett. **70**, 2621 (1993); G. Blatter, B. Ivlev, Y. Kagan, M. Theunissen, Y. Volokitin, and P. Kes, Phys. Rev. B **50**, 13013 (1994).
[8] A. Rozhkov and D. Stroud, Phys. Rev. B **54**, R12697 (1996).
[9] T. Onogi and S. Doniach, Solid State Commun. **98**, 1 (1996).
[10] A. Kramer and S. Doniach, Phys. Rev. Lett. **81**, 3523 (1998).
[11] S. Ryu, S. Doniach, G. Deutscher, and A. Kapitulnik, Phys. Rev. Lett. **68**, 710 (1992).
[12] T. Sasaki, W. Biberacher, K. Neumaier, W. Hehn, K. Andres, and T. Fukase, Phys. Rev. B **57**, 10889 (1998).
[13] M. M. Mola, S. Hill, J. S. Brooks, and J. S. Qualls, Phys. Rev. Lett. **86**, 2130 (2001).
[14] T. Sasaki, T. Fukuda, T. Nishizaki, T. Fujita, N. Yoneyama, N. Kobayashi, and W. Biberacher, Phys. Rev. B **66**, 224513 (2002).
[15] T. Sasaki, T. Fukuda, N. Yoneyama, and N. Kobayashi, Phys. Rev. B **67**, 144521 (2003).
[16] A. E. Koshelev, Phys. Rev. Lett. **83**, 187 (1999); Phys. Rev. B **68**, 094520 (2003).
[17] H. Urayama, H. Yamochi, G. Saito, K. Nozawa, T. Sugano, M. Kinoshita, S. Sato, K. Oshima, A. Kawamoto, and J. Tanaka, Chem. Lett. **17**, 55 (1988).
[18] C. Rossel, P. Bauer, D. Zech, J. Hofer, M. Willemin, and H. Keller, J. Appl. Phys. **79**, 8166 (1996).
[19] J. Muller, M. Lang, F. Steglich, J. A. Schlueter, A. M. Kini, and T. Sasaki, Phys. Rev. B **65**, 144521 (2002).
[20] M. Lang, F. Steglich, N. Toyota, and T. Sasaki, Phys. Rev. B **49**, 15227 (1994).
[21] F. Zuo, J. S. Brooks, R. H. McKenzie, J. A. Schlueter, and J. M. Williams, Phys. Rev. B **61**, 750 (2000).
[22] M. Tinkham, Phys. Rev. **129**, 2413 (1963).
[23] J. Singleton, J. A. Symington, M.-S. Nam, A. Ardavan, M. Kurmoo, and P. Day, J. Phys.: Condens. Matter **12**, L641 (2000).
[24] M. Lang, N. Toyota, T. Sasaki, and H. Sato, Phys. Rev. Lett **69**, 1443 (1992).
[25] S. Uji, K. Kodama, K. Sugii, T. Terashima, Y. Takahide, N. Kurita, S. Tsuchiya, M. Kimata, A. Kobayashi, B. Zhou, and H. Kobayashi, Phys. Rev. B **85**, 174530 (2012).
[26] M. M. Mola, J. T. King, C. P. McRaven, S. Hill, J. S. Qualls, and J. S. Brooks, Phys. Rev. B **62**, 5965 (2000).
[27] S. L. Lee, F. L. Pratt, S. J. Blundell, C. M. Aegerter, P. A. Pattenden, K. H. Chow, E. M. Forgan, T. Sasaki, W. Hayes, and H. Keller, Phys. Rev. Lett **79**, 1563 (1997).
[28] L. Yin, M.-S. Nam, J. G. Analytis, S. J. Blundell, A. Ardavan, J. A. Schlueter, and T. Sasaki, Phys. Rev. B **76**, 014506 (2007).
[29] T. Nishizaki, T. Sasaki, T. Fukase, and N. Kobayashi, Phys. Rev. B **54**, R3760 (1996).
[30] R. Kleiner and P. Muller, Phys. Rev. B **49**, 1327 (1994).
[31] J. U. Lee, J. E. Nordman, and G. Hohenwarter, Appl. Phys. Lett. **67**, 1471 (1995).
[32] W. K. Kwok, J. A. Fendrich, C. J. van der Beek, and G. W. Crabtree, Phys. Rev. Lett. **73**, 2614 (1994).
[33] V. F. Correa, G. Nieva, and F. de la Cruz, Phys. Rev. Lett. **87**, 057003 (2001).